Experimental Study of Effects of Forebody Geometry on High Angle-of-Attack Stability

Jay M. Brandon* and Luat T. Nguyen†
NASA Langley Research Center, Hampton, Virginia

A series of low-speed wind-tunnel tests on a generic airplane model with a cylindrical fuselage are made to investigate the effects of forebody shape and fineness ratio, and fuselage/wing proximity on static and dynamic lateral/directional stability. During the stability investigation ten forebodies were tested including three different cross-sectional shapes with fineness ratios of 2, 3, and 4. In addition, the wing was tested at two longitudinal positions to provide a substantial variation in forebody/wing proximity. Conventional force tests were conducted to determine static stability characteristics, and single-degree-of-freedom free-to-roll tests were conducted to study the wing rock characteristics of the model with the various forebodies. Flow visualization data were obtained to aid in the analysis of the complex flow phenomena involved. The results show that the forebody cross-sectional shape and fineness ratio and forebody/wing proximity can strongly affect both static and dynamic (roll) stability at high angles of attack. These characteristics result from the impact of these factors on forebody vortex development, the behavior of the vortices in sideslip, and their interaction with the wing flowfield.

Nomenclature

b = wing span, ft
c = mean aerodynamic chord length, ft
C_L = lift coefficient
C_ℓ = rolling-moment coefficient
$\hat{C}_\ell$ = estimated rolling-moment coefficient
C_{ℓ_β} = lateral-stability derivative, $\frac{\partial C_\ell}{\partial \beta}$, deg^{-1}
C_{ℓ_p} = roll-damping coefficient, $\frac{\partial C_\ell}{\partial\left(\frac{pb}{2V}\right)}$, rad^{-1}
C_m = pitching-moment coefficient
C_n = yawing-moment coefficient
C_{n_β} = directional-stability derivative, $\frac{\partial C_n}{\partial \beta}$, deg^{-1}
I_x = roll moment of inertia, slug-ft
p = roll rate, rad/s
q = dynamic pressure, psf
S = wing area, ft^2
V = freestream velocity, ft/s
α = angle of attack, deg
α_o = angle of attack at $\phi = 0$ deg, deg
β = angle of sideslip, deg
ϕ = roll angle, deg

Introduction

NUMEROUS studies have shown that the forebody aerodynamics can dominate the stability characteristics of aircraft at high angles of attack.[1-6] In addition, it has been observed that some forebody geometries that provide favorable static stability characteristics can cause dynamic instabilities due to loss of yaw damping.[7] More recently, studies have shown that forebody aerodynamics can also strongly affect dynamic roll stability.[8,9] Loss of roll damping at high angles of attack can lead to wing rock, which is an undesirable sustained oscillation, primarily in roll, exhibited by many modern aircraft.

A research program is underway at the NASA Langley Research Center to provide a systematic low-speed wind-tunnel data base on the effects of forebody geometry on aircraft static and dynamic stability at high angles of attack. The primary goal of these studies is to advance understanding of the complex flow phenomena involved at high angle-of-attack flight conditions. Research is focusing on wind-tunnel studies of a very simple generic airplane model with geometry flexibility. This geometric flexibility allows investigation of primary design factors including forebody cross-sectional shape and fineness ratio, wing planform and location, and empennage geometry. Results from the first series of tests of this model were reported in Ref. 9 and showed that forebody/wing flow coupling can dominate the static and dynamic stability near stall. To further explore this phenomenon, a current study is focused on the effects of forebody length and forebody/wing proximity. Forebody length was varied by testing specific forebody shapes over a range of fineness ratios, while forebody/wing proximity was investigated by moving the wing longitudinally along the fuselage. This paper will review some of the results of these tests.

Model and Tests

Wind-tunnel tests were conducted on a generic airplane model with variable geometry. The model consists of a very simple cylindrical fuselage on which a number of different wings, forebodies, and tails can be mounted. To study the effect of cross-sectional shape on stability, tests were conducted on forebodies with horizontal elliptical, vertical elliptical, and circular cross-sectional shapes. The corresponding ellipticity ratios (ratio of height to width) of these forebodies were 0.625, 1.6, and 1, respectively. Figure 1 presents a comparison of the different forebody cross-sectional shapes tested. To investigate the effect of fineness ratio on stability, each cross-sectional shape forebody was tested at three different lengths corresponding to fineness ratios of 2, 3, and 4. In an effort to test a "forebody removed" configuration, a blunt hemispherical cap

Presented as Paper 86-0331 at the AIAA 24th Aerospace Sciences Meeting, Reno, NV, Jan. 6-9, 1986; received Oct. 14, 1986; revision received Jul. 7, 1987.

*Aerospace Engineer.
†Assistant Head, Flight Dynamics Branch.

nose was also investigated. Thus, a total of ten forebodies were tested. These forebodies were mounted to a simple cylindrical fuselage and the test configuration was completed with the addition of a flat plate trapezoidal wing with a 26-deg leading-edge sweep angle and sharp beveled leading and trailing edges. Vertically, the wing was attached to the fuselage at its centerline, thus giving a midwing position. Longitudinally, the wing was mounted at two positions as shown in Fig. 2. At the nominal location, the wing apex was 15.3 in. behind the forebody. At the forward position, the wing was moved 15.3 in. forward such that the apex was located at the forebody-fuselage juncture. The reason for testing this configuration was to assess the effect of forebody/wing proximity on the coupling of the respective flowfields that in turn can dominate roll stability at high angles of attack. It should be noted that with the wing in the forward position, the moment reference center was also moved such that it remained at the wing quarter chord. In doing this, however, the distance from the forebody to the reference center was greatly reduced and the length of the aft fuselage was increased significantly as shown in Fig. 2. The resulting impact on pitching and yawing moment would be expected to be large, particularly at the higher angles of attack. It is important to keep this fact in mind when comparing the static data for the two wing positions.

Static, free-to-roll, and flow visualization tests were conducted in the Langley 12-ft low-speed wind tunnel. The static force and free-to-roll tests were performed at a dynamic pressure of 5 psf, resulting in a Reynolds number of 0.26×10^6 based on the fuselage diameter. Conventional force and moment data were obtained over an angle-of-attack range of 0–50 deg at angles of sideslip of up to 20 deg. For use in analysis of the free-to-roll results, static force data were also obtained at angle of attack and sideslip conditions that correspond to roll angles experienced during wing rock motions. As indicated earlier, all measurements were referenced to a moment center located at the 25%c location of the wing.

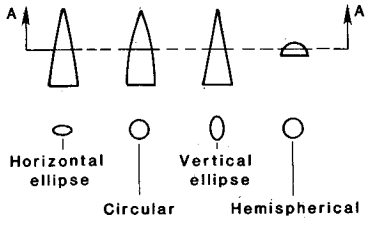

Fig. 1 Forebody cross-sectional shapes tested.

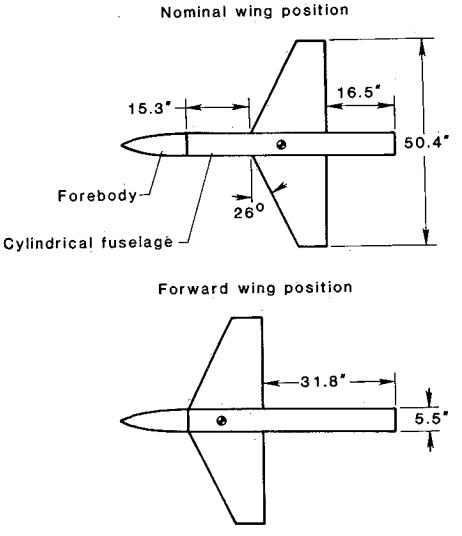

Fig. 2 Wing positions tested.

The free-to-roll test was the primary test technique used to investigate the wing rock tendencies of the study configurations. In the free-to-roll tests the model was mounted on an apparatus consisting of two concentric barrels attached by ball bearing assemblies that allowed the model to rotate freely about its roll axis. Roll angle time history data measured by a potentiometer were recorded and numerically differentiated to obtain values of the roll rate and acceleration during wing rock conditions. An estimate of the aerodynamic rolling moment coefficient acting on the model during the motions was then obtained from the relationship $C_\ell = I_x\ddot{\phi}/qSb$. The roll inertia of the model was experimentally determined using a conventional oscillation technique. More information about the free-to-roll test technique may be found in Ref. 10. To aid in analysis of the static and free-to-roll results, flow visualization was obtained by injecting smoke at appropriate locations in the tunnel.

Static Stability Characteristics

Effect of Forebody Cross-Sectional Shape

Data to be discussed in this section will be for configurations with the nominal wing position and forebodies of fineness ratio = 3. The variations of the measured lift and pitching moments for the three forebody shapes (horizontal ellipse, vertical ellipse, and circular) and the forebody off configuration are presented in Fig. 3. The data show reductions in lift curve slope above about 10 deg angle of attack, which is indicative of

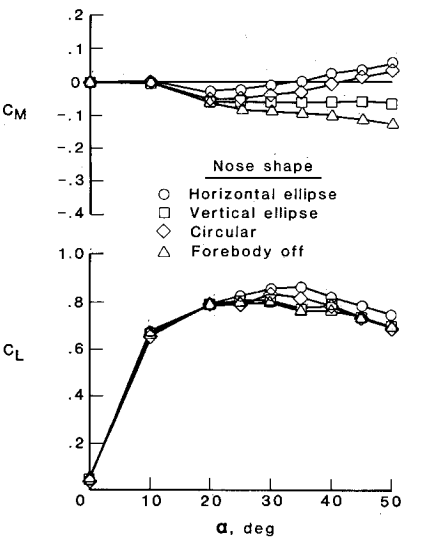

Fig. 3 Effect of forebody cross-sectional shape on longitudinal stability (fineness ratio = 3; nominal wing position).

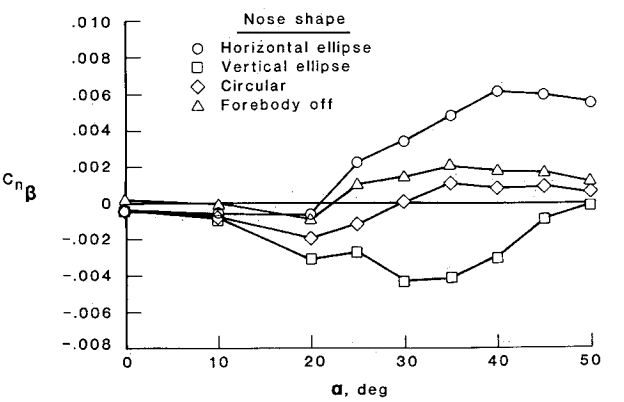

Fig. 4 Effect of forebody cross-sectional shape on directional stability (fineness ratio = 3; nominal wing position).

wing stall progression. Above $\alpha = 20$ deg, the forebody aerodynamics become more dominant as suggested by the increase in lift compared to the forebody off configuration. Maximum lift is obtained near $\alpha = 30$ deg. The corresponding pitching moment data also indicate a significant effect of the forebody cross-sectional shape above $\alpha = 20$ deg. The data show that the vertical ellipse configuration exhibits the highest pitch stability, followed by the circular and horizontal ellipse configurations. This inverse relationship between lift and pitch stability indicates that the forebody vortices are acting on the forebody and other areas ahead of the reference center to produce additional lift and nose-up pitching moment increments.

Static directional stability results for the different nose shapes and for "forebody-off" condition are summarized in Fig. 4. The data were obtained by sloping the measured yawing moment coefficient data between ± 5 deg of sideslip. Below 20 deg angle of attack, the directional stability for all forebody shapes is slightly negative since the model did not incorporate a vertical tail. Above $\alpha = 20$ deg, where the forebody vortex flows become strong, a large variation in directional stability levels is observed ranging from very stable for the horizontal ellipse nose to very unstable for the vertical ellipse nose. The results shown are generally consistent with results reported from previous studies. Figures 5–7 show sketches of the primary vortex positions above the three forebodies based on observations at $\alpha = 30$ deg using the smoke flow visualization technique. Figure 5 depicts the flow around the horizontal ellipse forebody. At $\beta = 0$ deg, a pair of vortices is located essentially symmetrically above the forebody. At sideslip, the windward vortex moves inboard but remains close to the body surface and displaces the leeward vortex vertically away from the nose. This creates a force on the forebody that tends to reduce the sideslip. Additionally, the primary flow separation points remain near the maximum half-breadth of the forebody in sideslip. The flow pattern around the circular nose is similar to that of the horizontal ellipse nose (Fig. 6); however, the windward primary separation point moves further up on the body resulting in the windward vortex positioned beyond the centerline of the nose. Also, there is no significant displacement of the leeward vortex away from the surface of the body. The net result of these flow characteristics is that no substantial sideforce is generated on the nose. The position of the forebody vortices in sideslip is further altered by the progression to the vertical ellipse cross-sectional shape as shown in Fig. 7. With this forebody, the leeward vortex positions itself underneath the windward vortex and stays close to the nose surface, producing a destabilizing suction force on the nose opposite to that observed for the horizontal ellipse forebody.

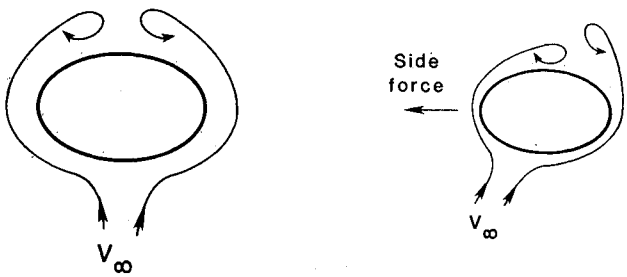

Fig. 5 Flow pattern above horizontal ellipse forebody ($\alpha = 30$ deg).

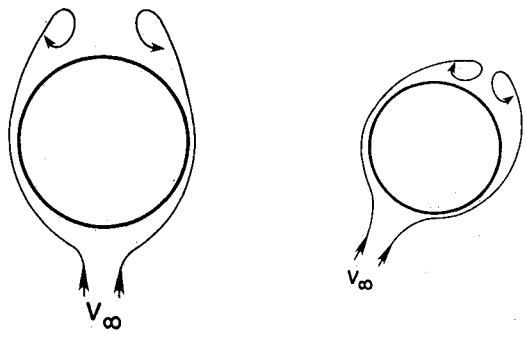

Fig. 6 Flow pattern above circular forebody ($\alpha = 30$ deg).

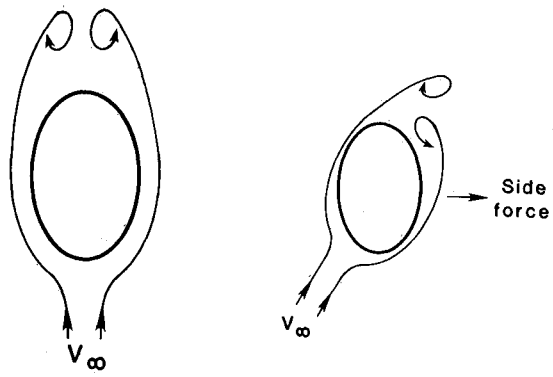

Fig. 7 Flow pattern above vertical ellipse forebody ($\alpha = 30$ deg).

Static lateral stability for the configuration with the three nose shapes and the "forebody-off" condition is summarized in Fig. 8. The data indicate that for this wing configuration, forebody cross-sectional shape also strongly influences C_{ℓ_β} at high angle of attack. Compared to the "forebody-off" case, the horizontal ellipse shape again has a stabilizing effect, whereas the vertical ellipse and circular noses are detrimental to stability. The differences in stability levels for the different forebodies occurred primarily in the angle of attack range of 20–40 deg, which suggest a significant interaction of the forebody flowfield with the wing flowfield in this region. In the low angle-of-attack region below 20 deg, the forebody vortex system has not yet developed fully, and in the high angle-of-attack region ($\alpha > 40$ deg) the forebody and wing flowfields are no longer strongly coupled.

Effect of Fineness Ratio and Forebody/Wing Proximity

As indicated earlier, the primary reason for conducting tests with the wing in the forward position was to examine the effect on the forebody/wing flowfield interaction and the resulting impact on static and dynamic roll stability, In this section, static data will be presented for the configurations with the two wing positions incorporating the horizontal and vertical ellipse forebodies with fineness ratios of 2, 3, and 4.

Static directional stability results are summarized in Figs. 9 and 10. Figure 9 indicates that, for a fixed wing position, an increase in fineness ratio adds a positive increment in directional stability for the horizontal ellipse forebody configurations. This is the result of a combination of increased vortex

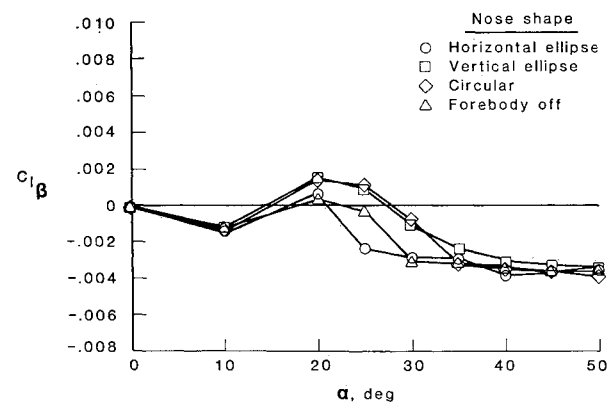

Fig. 8 Effect of forebody cross-sectional shape on lateral stability (fineness ratio = 3; nominal wing position).

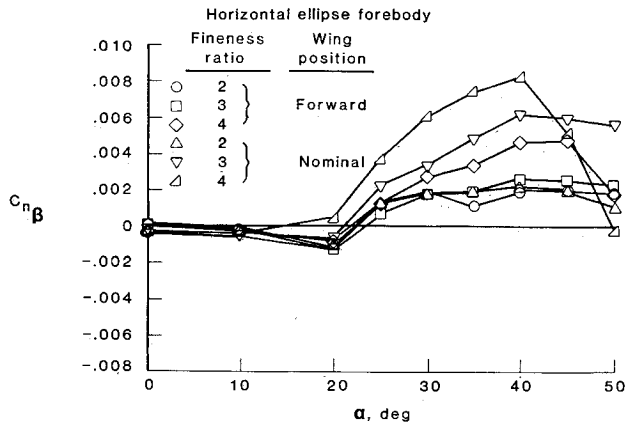

Fig. 9 Effect of fineness ratio and wing proximity on directional stability. Horizontal ellipse forebody.

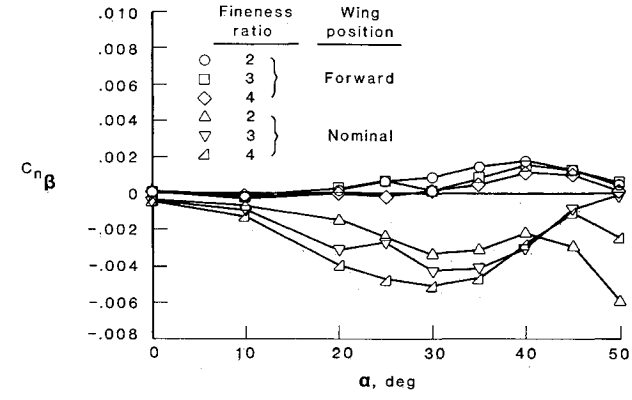

Fig. 10 Effect of fineness ratio and wing proximity on directional stability. Vertical ellipse forebody.

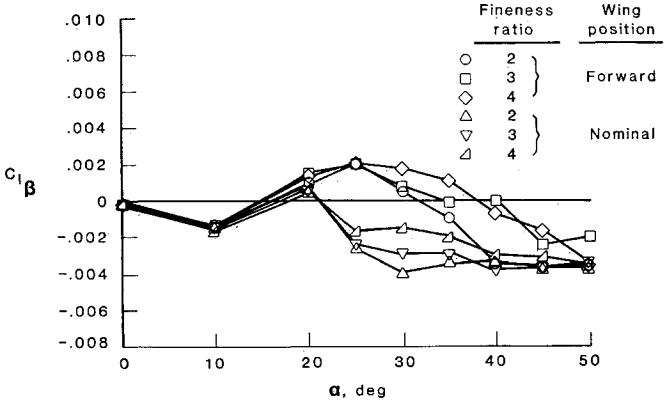

Fig. 11 Effect of fineness ratio and wing proximity on lateral stability. Horizontal ellipse forebody.

strength and increased moment arm for the stabilizing forces generated on the forebody. Moving the wing to the forward position produces a significant reduction in directional stability above 20 deg angle of attack due to the reduced forebody moment arm.

Figure 10 summarizes the results obtained for the vertical ellipse forebody. The data show a degradation in directional stability due to increased fineness ratio. This result is analogous to the previous result for the horizontal ellipse forebody. As discussed earlier, the flow pattern produced by the vertical ellipse forebody generates a destabilizing force. The effect of

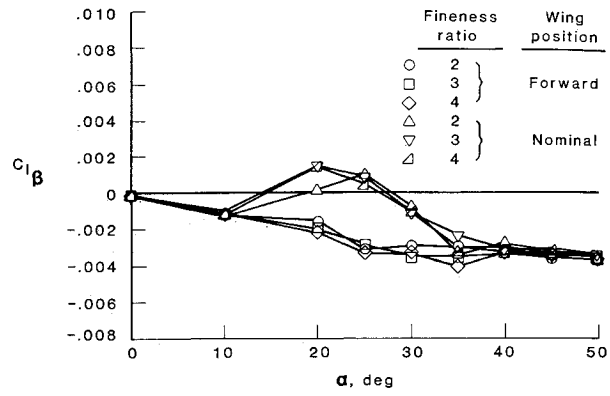

Fig. 12 Effect of fineness ratio and wing proximity on lateral stability. Vertical ellipse forebody.

this force is magnified with the larger fineness ratios due to the increased distance to the moment reference center. Moving the wing forward results in a substantial increase in directional stability because of the reduction in forebody moment arm.

Static lateral stability data are summarized in Figs. 11 and 12. Figure 11 presents results for the horizontal ellipse forebody shapes. The data indicate that for a given wing position, increasing the forebody fineness ratio decreases lateral stability at the higher angles of attack. Also, movement of the wing to a forward position produces a significant reduction in stability above $\alpha = 20$ deg. Thus, it appears that bringing the wing closer to the forebody allows the forebody flowfield to interact more strongly with the wing and adversely affect C_{ℓ_β}. The data show that the wing position effect is much stronger than the effect due to forebody fineness ratio. For example, at $\alpha = 30$ deg, moving the wing forward results in a variation from highly stable to moderately unstable regardless of forebody length.

Figure 12 summarizes the effect of forebody length and wing location on C_{ℓ_β} for the vertical ellipse forebody configurations. For a given wing position, it is seen that the variations in fineness ratio have very small effects on the static lateral stability. On the other hand, forebody-wing proximity strongly influences the values of C_{ℓ_β} for angles of attack between 15 and 35 deg. The results show that moving the wing closer to the forebody significantly enhances lateral stability, which is exactly opposite the effect observed for the horizontal ellipse configurations.

Figure 13 presents photographs of smoke flow visualization taken at $\alpha_o = 35$ deg with the model rolled approximately 10 deg right wing down. The wing was in the forward location and the model was fitted with fineness-ratio 3 noses. Smoke was injected at the wing root on the leeward side. With the horizontal ellipse configuration, the smoke flows show that the leeward forebody vortex passed over the inboard section of the left wing augmenting lift on the wing. This leeward wing lift contributed to the unstable lateral stability exhibited by this configuration. In contrast, the vertical ellipse configuration developed a leeward vortex that passed over the fuselage and was situated over the windward wing root. As a result, a lift increment was produced on the windward wing that provided lateral stability.

Dynamic Roll Stability

Effect of Forebody Cross-Sectional Shape

Free-to-roll results for the configuration showed that wing rock oscillations of varying amplitudes were exhibited by most of the configurations between 25 and 40 deg angle of attack. In this angle-of-attack range, the model began a roll oscillation without any external disturbance beyond the inherent turbu-

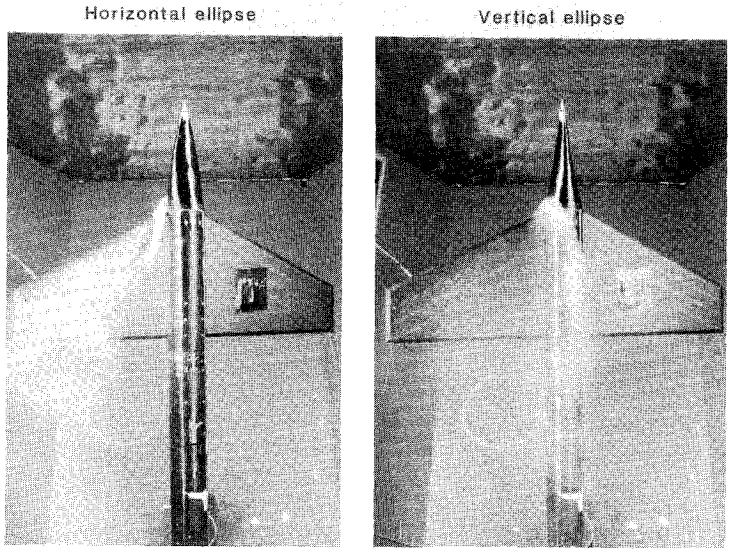

Fig. 13 Flow visualization over leeward wing ($\alpha_o = 35$ deg, $\phi = 10$ deg; forebody fineness ratio = 3).

lence of the tunnel. This characteristic is illustrated in Fig. 14, which presents a time history of the roll angle of the model with the horizontal ellipse nose with fineness ratio of 3. The model was released from an initial stationary position at $\alpha_o = 35$ deg and $\phi = -6$ deg. It is seen that a large amplitude wing rock motion built up rapidly over two to three oscillation cycles and that the "steady-state" oscillations were somewhat irregular with significant amplitude variations from cycle to cycle.

A summary of the free-to-roll results for the various nose shapes for a fineness ratio of 3 with the nominal wing position is presented in Fig. 15 in terms of observed oscillation amplitude vs angle of attack. These results indicate a significant effect of forebody cross-sectional shape on wing rock characteristics. The vertical ellipse nose shape was the most resistant to wing rock, exhibiting only small amplitude oscillations between 25 and 30 deg angle of attack. The horizontal ellipse forebody produced the largest amplitude of wing rock with amplitudes reaching $\Delta\phi = 40$ deg. Correlating these results to the static lateral stability data shown in Fig. 8, a trend is observed that the nose shapes that provide the highest levels of static stability also tend to cause the highest amplitude of wing rock and vice versa.

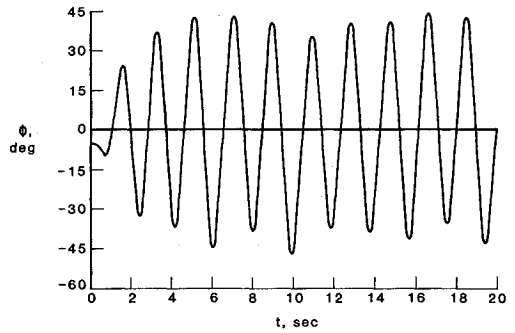

Fig. 14 Time history of wing rock buildup. Horizontal ellipse forebody ($\alpha_o = 35$ deg; fineness ratio = 3; nominal wing position).

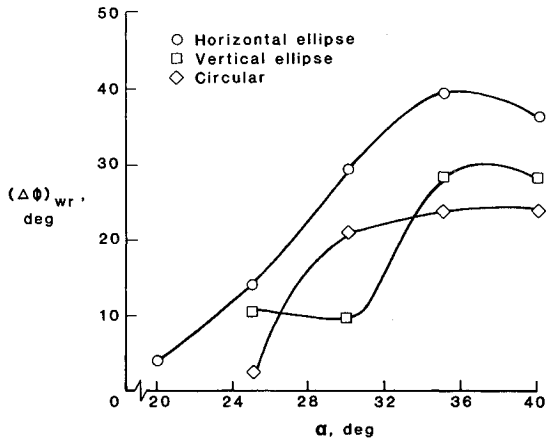

Fig. 15 Effect of forebody cross section on wing rock amplitude (fineness ratio = 3; nominal wing position).

Effect of Fineness Ratio and Forebody/Wing Proximity

The effect of forebody length on wing rock amplitude is illustrated in Fig. 16. Shown are data obtained at $\alpha_o = 35$ deg for the various forebody shapes at fineness ratios of 2, 3, and 4. The results indicate that forebody length can significantly influence wing rock amplitude. However, attempts at correlating these data with the static stability data did not define any consistent trends.

Wing rock data for the wing in the forward position are summarized in Fig. 17. These results should be compared to those of Fig. 15 to assess the impact of forebody/wing proximity. It is seen that moving the wing forward dramatically altered the wing rock characteristics. For example, with the wing in the nominal position, the horizontal ellipse configuration exhibited large amplitude wing rock above 25 deg angle of attack. On the other hand, the vertical ellipse configuration showed only small amplitude oscillations for angles of attack up to 30 deg. These characteristics are completely reversed with the wing in the forward position. The horizontal ellipse configuration became extremely resistant to wing rock, whereas the vertical ellipse configuration exhibited very large amplitude wing rock between 20 and 40 deg angle of attack. It is interesting to correlate these results to the static lateral stability discussed earlier. A clear trend is apparent, that while moving the wing forward (thus, bringing it closer to the forebody) reduced static lateral stability, it also reduced wing rock amplitude and vice versa. This result is illustrated in Fig. 18, which presents a cross plot of C_{ℓ_β} and $\Delta\phi$ for the horizontal and vertical ellipse configurations with the two wing positions at $\alpha_o = 30$ deg. The trend indicated in the plot also reinforces the earlier observation that configurations having the highest levels of static stability also tend to exhibit the largest amplitude of wing rock; whereas, configurations that have no static stability are wing-rock resistant.

Aerodynamic Moments during Wing Rock

As discussed earlier, estimates of the aerodynamic rolling-moment coefficient during wing rock were made by differentiating the roll displacement signal. These data were used to examine the time-varying loads that drove the limit-cycle oscillations. As an example, results will be discussed for a configuration incorporating the fineness-ratio 4 vertical ellipse nose with the wing in the forward position. This configuration was found to exhibit large amplitude wing rock at $\alpha_o = 35$ deg, similar to that shown in Fig. 14. To aid in the analysis of these motions, static data were measured at the combinations of α and β corresponding to the roll angles encountered during the free-to-roll tests. The rolling-moment data are shown in Fig. 19 as a plot of C_ℓ vs ϕ. The results indicate high levels of stability (negative slope) for roll angles up to about ± 40 deg. It is interesting to note that the observed wing rock amplitude at this condition was approximately 45 deg. Figure 20 presents estimates of the rolling-moment coefficients obtained from the free-to-roll data plotted vs roll angle. Results are shown for three ranges of reduced roll rates: $pb/2V \approx 0$ and $pb/2V \approx \pm 0.026$. Comparison of the $pb/2V \approx 0$ data to the static wind-tunnel data shown in Fig. 19 indicates fairly good agreement, which provides a check of the validity of the estimated coefficients. Comparison of the $pb/2V \approx \pm 0.026$ and $pb/2V \approx 0$ data indicates that for the smaller roll angles ($\phi < 20$ deg), the dynamic rolling moment differs significantly from the static values. For positive roll rates, the dynamic values are consistently higher than static and, conversely, at negative roll rate the dynamic values are more negative than the static values, indicating unstable roll damping. At larger roll angles, the differences between static and dynamic rolling moment become less distinct. This behavior is similar to that postulated to cause the wing rock exhibited by slender delta wings as discussed in Ref. 10.

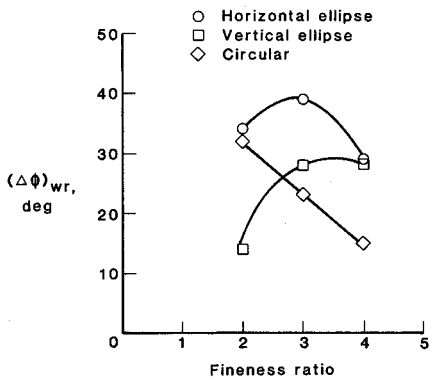

Fig. 16 Effect of forebody fineness ratio on wing rock amplitude ($\alpha_o = 35$ deg; nominal wing position).

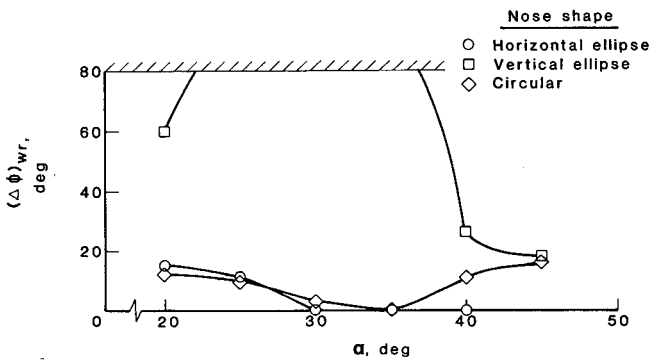

Fig. 17 Effect of forebody cross section on wing rock amplitude (fineness ratio = 3; forward wing position).

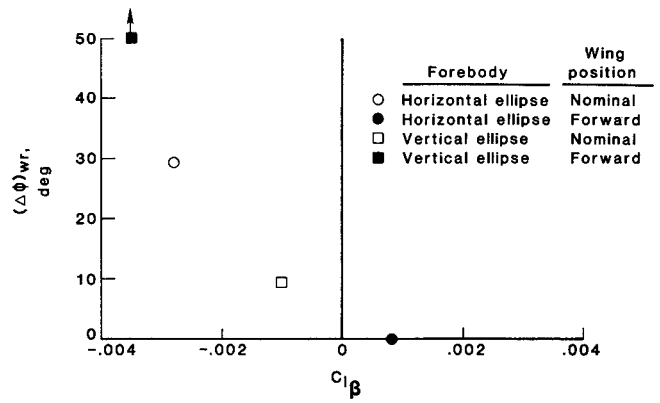

Fig. 18 Comparison of wing rock tendencies with static lateral stability ($\alpha_o = 30$ deg; forebody fineness ratio = 3).

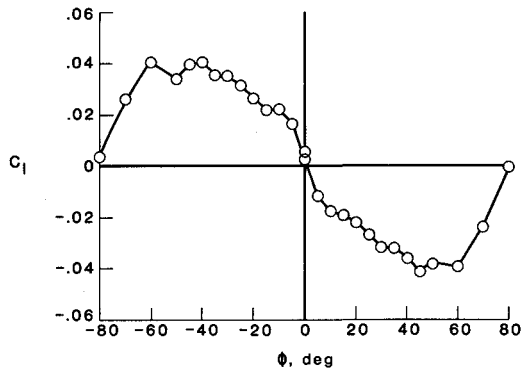

Fig. 19 Static rolling-moment coefficient at roll angle. Vertical ellipse forebody ($\alpha_o = 35$ deg; fineness ratio = 4; forward wing position).

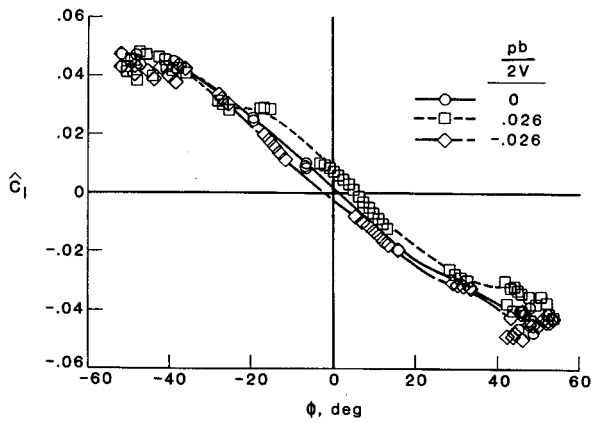

Fig. 20 Rolling-moment coefficient during wing rock. Vertical ellipse forebody ($\alpha_o = 35$ deg; fineness ratio = 4; forward wing position).

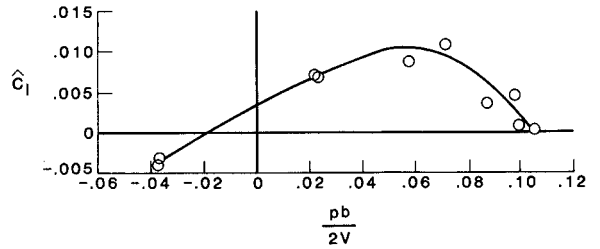

Fig. 21 Effect of roll rate on rolling moment during wing rock. Vertical ellipse forebody ($\phi = 0$ deg; fineness ratio = 4; forward wing position).

To further assess the variation of roll damping, Fig. 21 shows estimated rolling moment plotted vs reduced roll rate. The results were obtained by analyzing data at $\phi = 0$ deg over a large number of oscillation cycles. The plot indicates that at low rates, the roll damping is unstable, as shown previously in Fig. 20. Calculation of the slope gives a value of the roll damping parameter C_{ℓ_p} of 0.18. Additionally, however, the data show that at higher roll rates the damping becomes stable. The characteristic of unstable roll damping at small roll rates combined with stable damping at higher rates would promote the limit-cycle-type wing rock observed in the free-to-roll tests.

Conclusions

This paper has summarized recent research at the NASA Langley Research Center on the effects of forebody flows on static and dynamic stability at low-speed, high angle-of-attack conditions. The results of the stability tests show that:

1) Forebody cross-sectional shape and fineness ratio, and the proximity of the wing to the forebody can strongly affect static and dynamic stability in the angle-of-attack range around stall.

2) Cross-sectional shape and fineness ratio influence the development and strength of the forebody vortices, their behavior in sideslip, and their interaction with the wing flowfield.

3) Forebody/wing proximity directly affects the coupling of the two flowfields and as a result can profoundly influence static and dynamic roll stability at high angles of attack.

4) The combination of these factors produced static lateral/directional stability characteristics that ranged from highly stable to highly unstable, and configurations that were well damped in roll to those that exhibited very large amplitude wing rock.

5) A general trend was observed whereby configurations that had the highest levels of static lateral stability also tended to exhibit the largest-amplitude wing rock, whereas configurations that were statically unstable were very resistant to wing rock.

Follow-on tests are recommended to examine other configuration design factors including wing planform and placement and empennage geometry. In addition, more detailed flow visualization and measurements should be made to aid in analysis of the very complex flow mechanisms involved, particularly during wing rock. It is recognized that this set of data is being generated in wind-tunnel tests conducted at very low Reynolds number and that forebody separation phenomena are known to be Reynolds-number sensitive. High Reynolds number data will ultimately also have to be obtained in order to assess viscous effects and to allow confident application of the results to full-scale conditions.

References

[1]Grafton, S. B., Chambers, J. R., and Coe, P. L., Jr., "Wind Tunnel Free-Flight Investigation of a Model of a Spin Resistant Fighter Configuration," NASA TN D-7716, June 1974.

[2]Skow, A. M. and Erickson, G. E., "Modern Fighter Aircraft Design for High Angle-of-Attack Maneuvering," AGARD Lecture Series No. 121 on high angle-of-attack aerodynamics, March 1982.

[3]Carr, P. and Gilbert, W., "Effects of Fuselage Forebody Geometry on Low-Speed Lateral-Directional Characteristics of a Twin-Tail Fighter Model at High Angles of Attack," NASA TP 1592, 1979.

[4]Klein, J., Walch, K., and Hahne, D., "Airframe Component Effects on the Aerodynamic Stability and Control Characteristics of a Supersonic Cruise Fighter Aircraft at High Angles of Attack," AIAA Paper No. 84-2110, Aug. 1984.

[5]Erickson, G. and Gilbert, W., "Experimental Investigation of Forebody and Wing Leading-Edge Vortex Interactions at High Angles of Attack," *AGARD Conference Proceedings No. 342*, March 1984.

[6]Erickson, G. and Brandon, J., "Low-Speed Experimental Study of the Vortex Flow Effects of a Fighter Forebody Having Unconventional Cross-Section," AIAA Paper 85-1798-CP, Aug. 1985.

[7]Murri, D. G., Nguyen, L. T., and Grafton, S. B., "Wind Tunnel Free-Flight Investigation of a Model of a Forward-Swept-Wing Fighter Configuration," NASA TP 2230, 1984.

[8]Nguyen, L. T., Whipple, R. D., and Brandon, J. M., "Recent Experiences of Unsteady Aerodynamic Effects on Aircraft Flight Dynamics at High Angle of Attack," *AGARD Conference Proceedings No. 386*, Paper No. 28, 1985.

[9]Brandon, J. M. and Nguyen, L. T., "Experimental Study of Effects of Forebody Geometry on High Angle of Attack Static and Dynamic Stability," AIAA Paper 86-0331, Jan. 1986.

[10]Nguyen, L. T., Yip, L. P., and Chambers, J. R., "Self Induced Wing Rock of Slender Delta Wings," AIAA Paper 81-1883, Aug. 1981.